

Design of a 3D Vision-based Micro-Force Sensing Probe

Georges Adam and David J. Cappelleri

Abstract—This paper presents a vision-based micro-force sensing probe that is capable of μN level force sensing in three dimensions. The sensor is mounted on a standard micromanipulation probe and can be easily integrated into many systems. Furthermore, it is cheap, reliable, and can be specifically tailored for a desired application. Tests were conducted to demonstrate the accuracy of the system. It is capable of achieving sub- μN force resolution, with a range of 175 μN and an accuracy in the x, y, and z directions of 3.63%, 0.58%, and 0.61%, respectively. Two case studies using the vision-based micro-force sensing probe were performed to demonstrate the efficacy of the system.

Index Terms—Force sensing, micromanipulators, micro/nano robots

I. INTRODUCTION

The ability to sense forces at the microscale is extremely important for the development of new technologies and to expand the capabilities of micro systems. However, sensors at this scale are usually expensive and hard to implement. There are multiple methods that have been used to reach micro-Newton level resolution, such as capacitive MEMS sensors [1], piezoelectric sensors [2], [3], strain gauges [4], Atomic Force Microscope (AFM) measurements [5], [6], among others. Some possible applications of such sensors include the field of mechanobiology [7], theranostics [8], biomanipulation [9], and the automated assembly of micro parts. Additionally, force information can be used in parallel with haptic feedback devices [10] to allow for more precise manipulation.

In recent years, the field of micromanipulation has been gaining a lot of interest due to the ability of systems to accurately manipulate parts and perform automated assembly. With the increase in complexity of MEMS devices, there exists a need to assemble multiple microscale components together since microfabrication of a complex stand-alone micro device is usually expensive, extremely challenging, and even sometimes not possible. Adding a force-sensing capability to such micromanipulation systems will increase their range of applications as well as make current manipulation tasks even more precise. Another issue regarding micromanipulation is the uncertainties coming from the substrate where the manipulation occurs. At the microscale, surface forces play a large role and are extremely difficult to model and predict. In an effort to reduce the manipulation uncertainties that arise from surface forces, machine learning models can be used, as in [11]. With the addition of force feedback to the

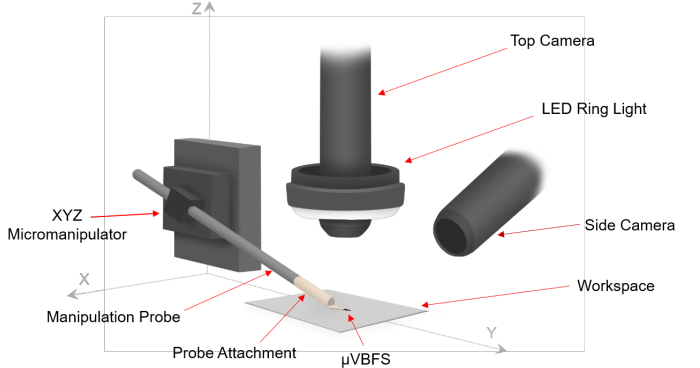


Fig. 1. Schematic of the 3D vision-based micro-force sensing probe. The microfabricated micro-scale vision-based force sensor (μVBFS) is attached to a manipulation probe. 3D deformation of the stiffness calibrated structure is captured by the dual camera vision system.

traditional micromanipulation setup, more accurate models can be developed. Additionally, it is also very desirable to create substrates that are able to minimize these uncertainties when pushing parts in the workspace. Micromanipulation of parts on these substrates with force feedback can help in their design.

A vision-based force sensor, which tracks the deflection of a stiffness calibrated compliant structure and uses the basic principles of Hooke's law to calculate force from displacement, can overcome many of the drawbacks associated with the use of AFM/capacitive sensors [12]–[14]. This compliant structure can be made out silicone elastometers with low Young's modulus and high failure strain, such as polydimethylsiloxane (PDMS), which allows for a high force sensing resolution and reliability. These systems have been used in a multitude of applications, both in one [15] and two dimensions [16]–[18].

In this paper, a proof of concept of a vision-based micro-force sensing probe capable of accurately measuring 3D micro-Newton level forces that can be easily integrated in standard micromanipulation test-beds is presented (Fig. 1). This sensor builds off of the work in [17] but adds an extra dimension of measurement, a decrease in sensor size, and an increase in sensitivity and resolution in all dimensions. Section II describes the overall design of the sensor and Section III described the fabrication. Then, Section IV addresses the sensor calibration, 3D vision tracking algorithm, and sensor validation studies. Lastly, Section V presents two case studies that showcase possible applications of the sensor and how it behaves during actual experiments.

*This work was supported by NSF NRI Award #1637961

Both authors are from the Multi-Scale Robotics and Automation Lab in the School of Mechanical Engineering at Purdue University, West Lafayette, IN, USA, 47907. {adamg, dcappell}@purdue.edu

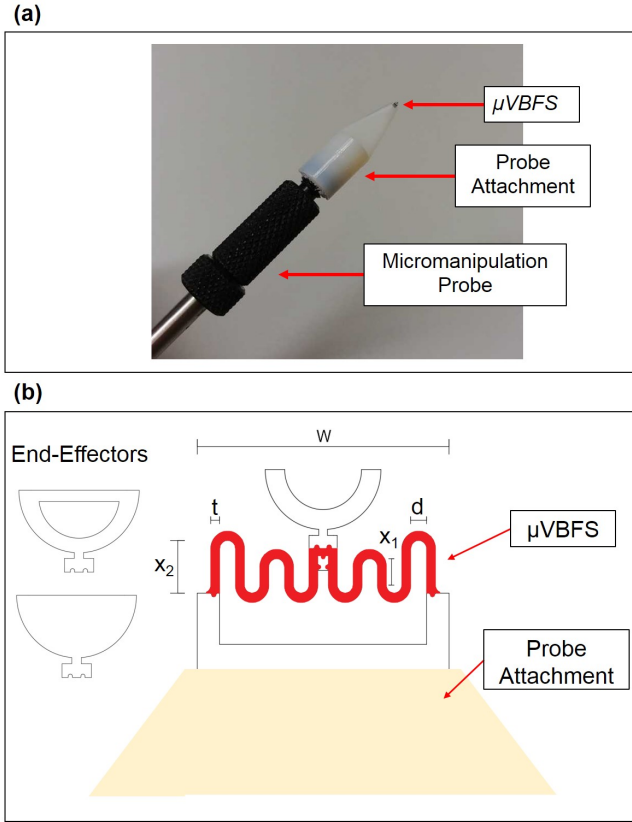


Fig. 2. 3D vision-based micro-force sensing probe: (a) final micro-sensor assembly, (b) overall design of μ VBFS with corresponding dimensions. Here, $t = 25$, $d = 45$, $W = 719$, $x_1 = 50$, and $x_2 = 122$, all in units of μm .

II. DESIGN OVERVIEW

For a vision-based force sensor, the sensed force in a particular direction, F_i , is determined by multiplying the stiffness in that direction, k_i , by the measured deflection, δ_i . This way, the lowest force detected corresponds to the smallest deflection detectable by the vision system. In order to make an accurate measurement, we assume that a minimum deflection of at least a pixel is needed to identify a corresponding deflection in microns. Therefore, there is a trade-off between the size of the field of view (FOV) and the minimum detectable force. For a larger FOV, each pixel corresponds to a larger physical distance, thus decreasing the minimum measurable deflection and therefore, the force.

The vision-based micro-force sensing probe is made up of three main parts, as shown in Fig. 2(a): 1. the manipulation probe, 2. the attachment fixture, and 3. the micro-scale vision-based micro-force sensor (μ VBFS). The probe attachment fixture is used to mount the sensor to a standard micromanipulation probe. This part has been 3D printed using a Connex3 350 Polyjet printer. The threaded part of the design can be simply screwed into a standard micromanipulation probe, which makes the sensor easily integratable into test-beds for many applications. On the other end of the fixture, there is a small slot used to attach the body of the μ VBFS.

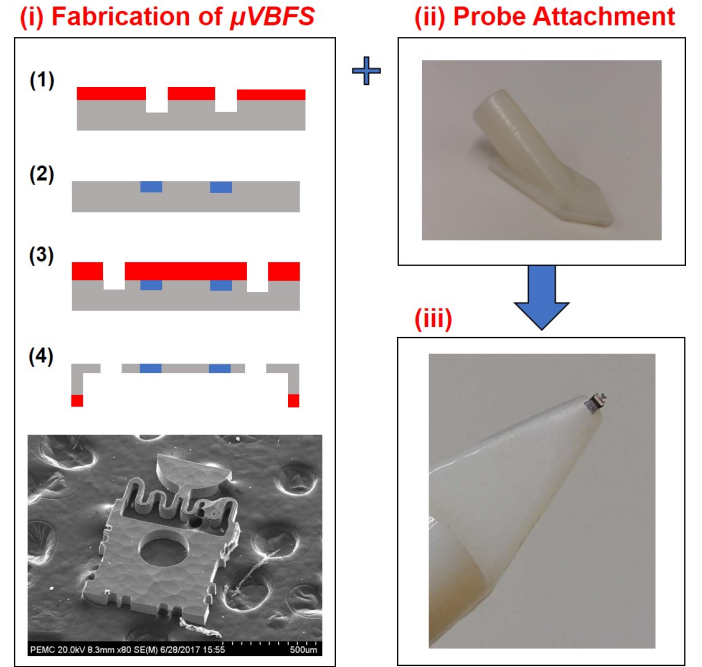


Fig. 3. Overall fabrication procedure of the 3D vision-based micro-force sensing probe. (i) Fabrication steps for making the μ VBFS: (1) Photolithography and etching to create the mold for the compliant structure; (2) the deposition of the PDMS structure; (3) the photolithography and etching to outline the rigid outer frame; and (4) the backside etching to release the sensor from the Si wafer. (ii) 3D printed probe attachment fixture; (iii) Final assembly of the μ VBFS to the fixture.

This allows the tip of the μ VBFS to interact with the objects being manipulated. Figure 2(a) shows the final assembly of the device.

In order to be able to measure μN -level forces, the stiffness of the compliant structure must be small enough so these forces will cause deflections within the detection range of the vision system. Due to these constraints, the compliant structure was made out of PDMS (Sylgard 184 silicone elastomer kit) with appropriate geometry to observe its deflection, as shown in Fig. 2(b).

III. SENSOR FABRICATION

The fabrication process of the μ VBFS was designed to allow for the creation of compliant structures with varying stiffness properties depending on the desired application. It is based on subsequent photolithography steps followed by a deep reactive-ion etch (DRIE), which creates both the mold where a PDMS structure will cure and the outer rigid frame of the sensor (Fig. 3). First, positive photoresist AZ1518 is spin coated at 1000 rpm for 30 seconds then it is soft-baked at 100°C for 3 minutes. The wafer is then exposed for 30 seconds using a Suss MA6 Mask Aligner (SUSS MicroTec), which creates the outline of the spring structure. The non-polymerized photoresist is then removed using MF CD-26 developer (Microchem Inc., USA) for 30 seconds, followed by a post-bake at 100°C for 3 minutes, and the DRIE process,

which is used to create the PDMS mold with the final desired thickness of the μ VBFS. In order to fabricate the compliant structure, PDMS is mixed at a base/curing agent ratio of 10:1 or 16.7:1, depending on the desired stiffness, and degassed for 30 minutes to remove air bubbles. The PDMS is then spin-coated onto the wafer at 2000 rpm for 30 seconds, and the excess polymer is removed using a silicone spatula. After the PDMS is cured for 24 hours at room temperature, the wafer is cleaned with acetone, leaving behind the compliant structures embedded into the silicon wafer. The μ VBFS frame is defined in a similar way. A photolithography process as described for the PDMS structure is performed but this time with a different mask. Then, the DRIE process will etch the silicon around the sensor frame. After another acetone cleaning step, the μ VBFS is ready to be released. A back-side window in patterned on the back of the wafer and the sensors are individually collected after a backside etching process, also using DRIE.

Once the μ VBFS fabrication is completed, each sensor's stiffness is individually calibrated in the x, y, and z directions (see Section IV-A). The sensor is then glued to the tip of the 3D printed probe attachment fixture. The fixture is then screwed into a micromanipulation probe. Since the fabrication process allows for the fabrication of sensors with different stiffness values, multiple force sensor/probe attachment pairs are created and they can easily be changed based on desired application and force ranges.

IV. VISION-BASED MICRO FORCE SENSOR CALIBRATION

There are two key components needed to develop an accurate vision-based micro-force sensor. The first is an accurate stiffness calibration of the PDMS compliant structure in all three dimensions. The second is the image processing algorithm used to measure the deflections of the sensor with relation to its body, also in three dimensions. Each of these critical steps are described in the subsections below.

A. Stiffness Calibration

In order to be able to measure forces in three dimensions using a vision-based method, it is necessary that the stiffness in the x, y, and z axis to be obtained (k_x , k_y , k_z , respectively). This was done by securing the μ VBFS to a glass slide and using a XYZ micromanipulator (MP-225, Sutter Instruments) to push a commercial force sensor (FT-S100, FemtoTools) against it. Figures 4(a-c), show the FT-S100 sensor pushing against the tip of the compliant structure with visible deflection. Multiple force measurements were obtained this way for different deflection amounts. This was repeated for each direction and the results plotted, as shown in Fig. 4(d). The stiffness is obtained by fitting a line to the data points and calculating its slope. As shown, for this specific sensor, the stiffness is: $k_x = 0.1206$ N/m, $k_y = 0.2422$ N/m, and $k_z = 0.0539$ N/m. For each of the curves, more than thirty data points were recorded.

Based on the results of this calibration, the resolution of the sensor in each direction, as well as range was calculated, as shown in Table I. In this case, the minimum resolution refers

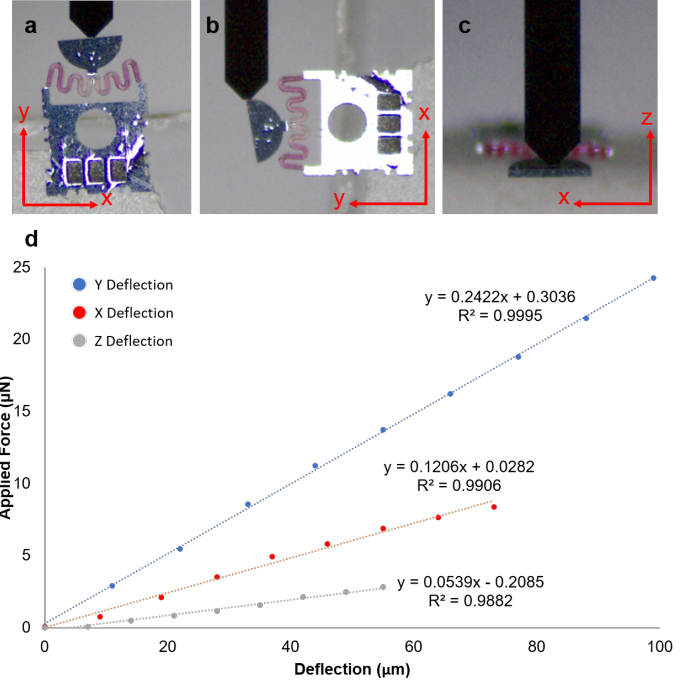


Fig. 4. Results from the 3D calibration of the μ VBFS. The slope of the curves correspond to the stiffness in the respective direction. The images shown in (a), (b), and (c) represent the deflections in the y, x, and z directions, respectively.

TABLE I
TABLE SUMMARIZING THE RESULTS OF DIFFERENT μ VBFS

Sensor	Direction	Stiffness (N/m)	Resolution (uN)	Range (uN)
Sensor 1	x	0.1206	0.8128	[0 17]
	y	0.2422	1.6324	[0 37]
	z	0.0539	0.3633	[0 6]
Sensor 2	x	0.1270	0.8560	[0 18]
	y	0.4148	2.7958	[0 63]
	z	0.0540	0.3640	[0 6]
Sensor 3	x	0.5364	3.6153	[0 73]
	y	1.2282	8.2781	[0 186]
	z	0.2008	1.3534	[0 20]

Note: the given resolution is based on the camera's zoom and its corresponding μ m/pixel ratio. The values here correspond to a FOV of 5.26×3.95 mm (3.29 μ m/pixel). The case studies were performed using a larger FOV (11.98 \times 8.98 mm and 7.49 μ m/pixel ratio).

to the minimum force measurable based on the camera pixel resolution (3.37 μ m/pixel for the top camera and 3.54 μ m/pixel for the side camera) and a displacement tracking accuracy of 1 pixel. Note that the camera pixel resolution depends on the size of the field of view for the 1600 \times 1200 pixel image. For calibrations, the image is zoomed in to have a more accurate measurements. The sensing range is the maximum force that can be measured before the compliant structure contacts the silicon frame. As seen, the stiffness can be tailored depending on the desired application, and the sensing range can go up to 175 μ N while obtaining close to sub- μ N force sensing resolution.

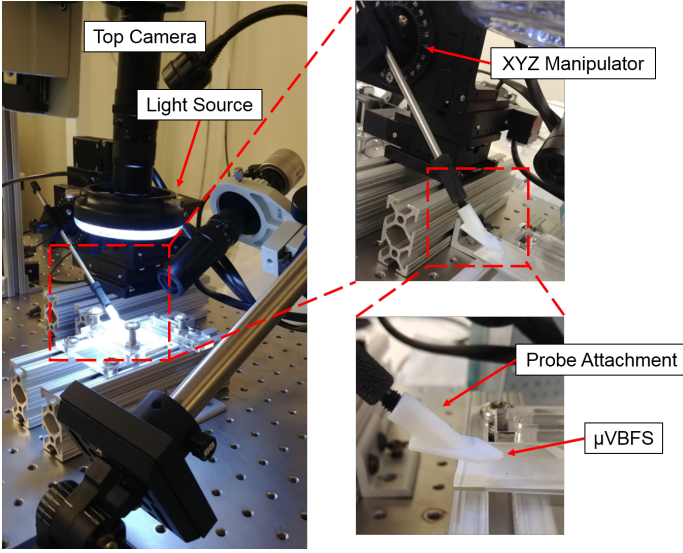


Fig. 5. Experimental setup used to record the videos and perform the manipulation tasks.

B. 3D Vision Tracking Algorithm

The goal of the vision tracking algorithm is to accurately measure the displacement of the compliant structure as the probe applies forces to other objects. The experimental setup, as shown in Fig. 5, contains two cameras (side and top views), the XYZ micromanipulator (MP-225, Sutter Instruments), and a custom made test-bed that keeps the working substrates secured during manipulation. Both cameras used are 1.3MP CMOS cameras (PointGrey e2v EV76C560) with adjustable magnifications ranging from 0.75x to 4.5x.

In order to measure the deflections of the compliant structure, an algorithm that uses multiple-object tracking techniques was employed. It keeps track of the positions of the tip of the end-effector and the μ VBFs body in two camera views. At first, two regions of interest (ROI's) are defined and the algorithm records their respective center positions over time (Fig. 6(a)). This creates a vector between the body and the end-effector tip for each camera view, which changes magnitude (length) and angle during the manipulation process. By tracking these changes and applying a transformation matrix, the deflection in the x, y, and z directions are computed. All of the tracking was performed offline using the Discriminative Correlation Filter Tracker with Channel and Spatial Reliability method [19] and the algorithm was able to run at 15 Hz. Since the stiffness of the compliant structure is known, these deflections are then used to compute the force applied in 3 dimensions, as intended. The custom developed application was written in Python using the OpenCV package (version 3.4.1).

C. Sensor Validation

In order to check the validity and accuracy of this tracking method, a fixed block was pushed multiple times using the probe at intervals of approximately $20\text{ }\mu\text{m}$ each, with a total displacement of exactly $80\text{ }\mu\text{m}$. This was done using the 3-axis micromanipulator, which has a $1\text{ }\mu\text{m}$ step size. Then,

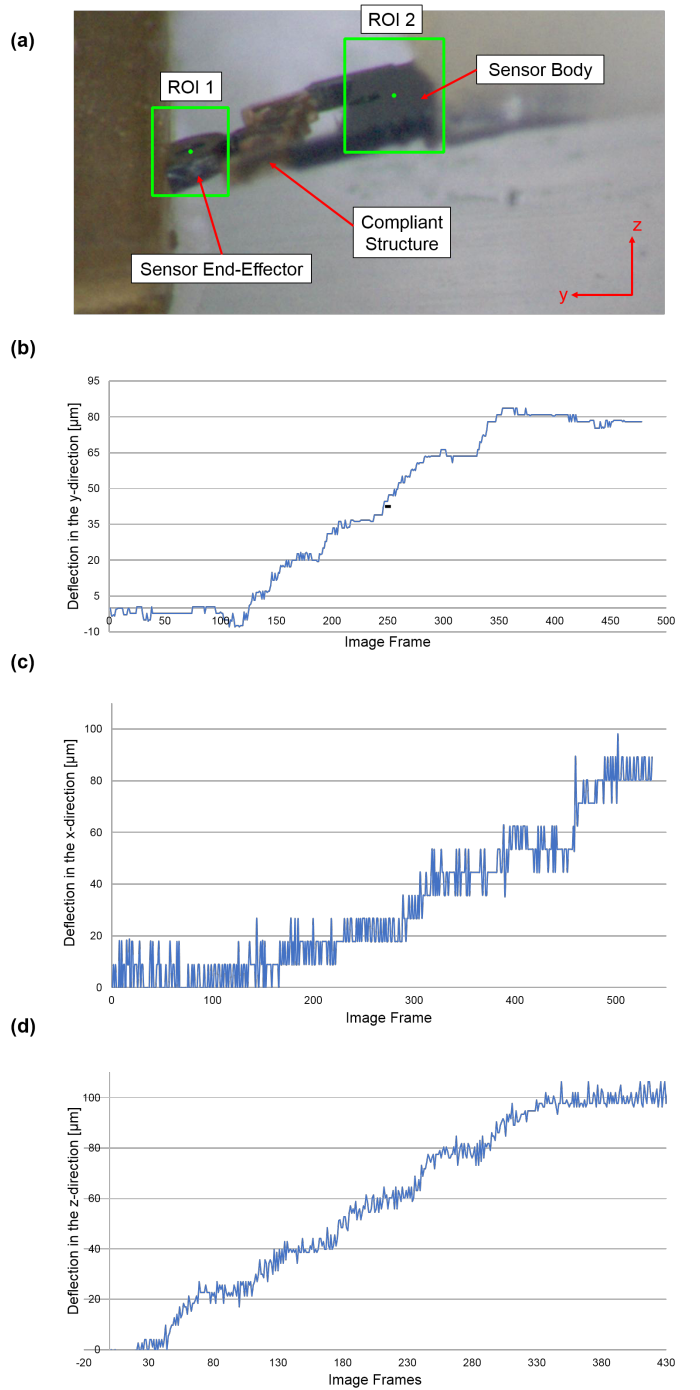


Fig. 6. Results of the sensor validation experiments showing the total displacement of the end-effector tip when compared to the body. (a) The locations of the ROIs from which the algorithm computes the deflections in the y and z directions. The resulting displacement plots for a simple pushing task in the (b) y-direction, (c) x-direction, and (d) z-direction.

using the 3D vision tracking algorithm described in Section IV-B, the measured deflection in all three axes was recorded. By comparing the measured values with the actual deflection (displacement), the accuracy of the vision-based micro-force sensor tracking algorithm can be validated.

Figure 6 shows the actual ROI tracking and the measured deflections in all three axes. As noted, the deflection increases in increments of $20 \mu\text{m}$ and remains stable at $80 \mu\text{m}$ at the end of the pushing validation. Clearly, both the x and y directions obtained displacement readings close to the nominal values, with an average final error of approximately 0.58% in the y-direction and 3.63% in the x-direction. For the validation in the z-direction, an extra $20 \mu\text{m}$ step was performed, so the total travel was $100 \mu\text{m}$, with an average final error of approximately 0.61%.

V. CASE STUDIES

Now that the μ VBFs has been validated, it can be used in various micromanipulation applications. In this section, two case studies are shown: (A) pushing of microscale blocks around the workspace with manipulation force extraction and (B) surface force measurement when manipulating micro-parts on different substrates. Both of these studies show possible applications of the μ VBFs and the range of experiments that can be performed with them.

A. Micromanipulation with Force Sensing

In a general sense, the probe developed here can be used for any micromanipulation application in which the pushing forces fall within the sensor's range. In order to put into perspective the capabilities of the 3D vision-based micro-force sensing probe, a simple manipulation task was performed with a silicon micro-block, as shown in Fig. 7. The goal is to move the micro object into a specific slot, similar to what would be done in a general microassembly procedure (peg-in-the-hole problem). The manipulation of part was performed manually. As a general procedure for this experiment, the part was pushed using the XYZ micromanipulator until it reached its goal location. While the manipulation was being performed, two cameras (top and side) recorded the entire workspace. The videos were then analyzed using the 3D vision tracking algorithm described in Section IV-B. Since the compliant structure used for the experiment had been previously calibrated, the stiffness value in each direction are known, and the algorithm can compute the forces applied in each direction during the entire manipulation process. Figure 7 also includes these extracted forces for this particular manipulation task. This case study shows the potential for using the μ VBFs for 3D closed-loop force controlled manipulation and assembly tasks in the future.

B. Measuring Surface Forces for Different Substrates

Pushing objects in the microscale is a rather uncertain task, since surface forces play a very large role in the results and are extremely hard to model. Any imperfection in the substrate lattice can cause different friction forces along the same surface. Additionally, even dust or small particles can have

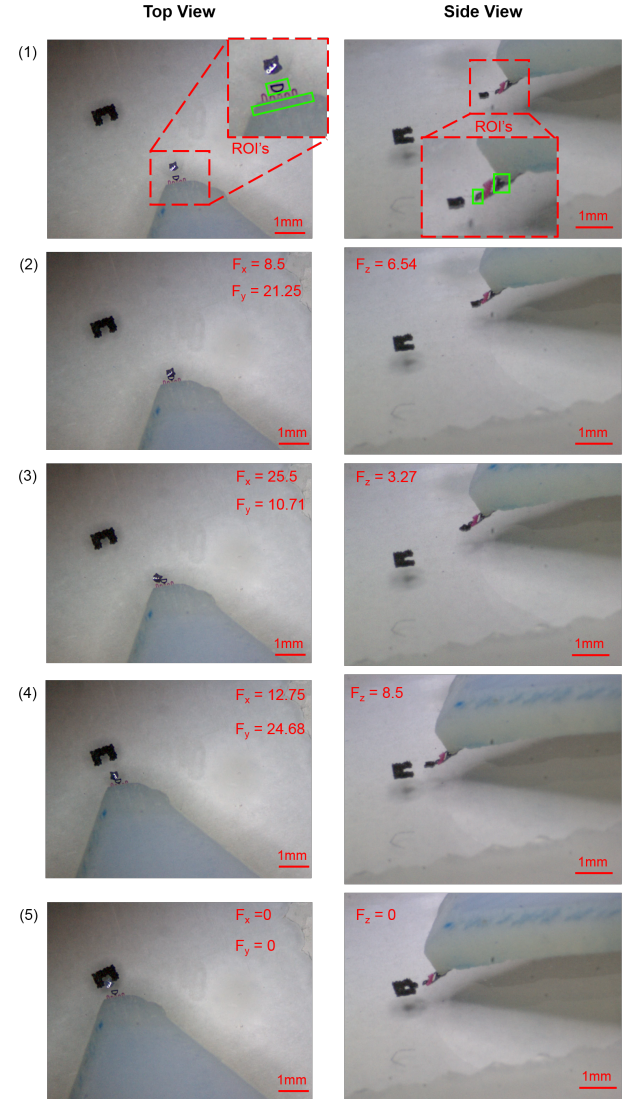


Fig. 7. Screenshots at different time stamps for the object manipulation from the initial (1) to final position (5) from both the top and side view with the measured forces at each moment.

a great effect in the manipulation process. Therefore, this case study aims to measure the necessary pushing forces required to manipulate the same object for different manipulation substrates to determine which can produce the most reliable manipulation surface. This is done by pushing a silicon micro-block across different surfaces while recording the necessary force to make the object move. Three substrates were tested: a glass slide, a glass slide cleaned using Isopropanol Alcohol (IPA), and a glass slide with a thin hydrophobic gold layer on its surface.

The hydrophobic coating was obtained by sputtering a thin 60 nm gold layer onto the glass slide and then placing it in a 0.5 mM solution of 1-Dodecanethiol (Sigma-Aldrich) in Ethanol Absolute (94-96%, Alfa Aesar) for 13 hours [20]. Figure 8 shows the magnitude of the resulting 3D force from pushing the same object across the three different substrates. In general, the average force needed to push the object

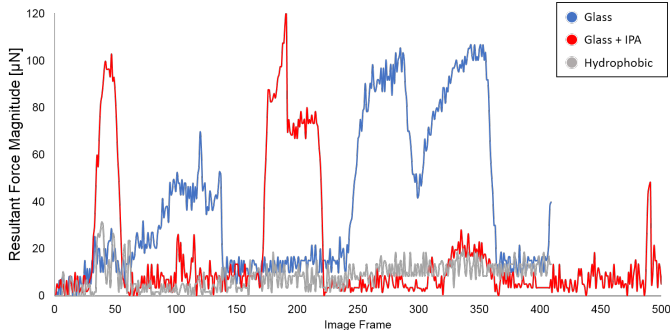


Fig. 8. Pushing force in the y-direction for different substrates using the same Silicon micro-block.

is approximately the same for all substrates. However, the glass slide and the glass slide with IPA displayed several unpredictable force peaks. These are due to the fact that the part encountered a region of the substrate in which the friction force was elevated, thus requiring a lot more force to move the object.

Comparing the glass slide with the IPA cleaned glass slide, both present two large peaks of approximately the same magnitude (approximately 100 μ N), while the regular glass slide has two extra 70 μ N peaks. Clearly, the hydrophobic gold surface is superior in reducing the uncertainties in the surface forces since it does not display any large force peaks during the pushing task. Therefore, the μ VBFs is able to identify and quantify this coating as a robust surface for planar micromanipulation tasks.

VI. CONCLUSIONS

In this paper, we have presented the proof-of-concept of a 3D vision-based micro-force sensor to be used in a standard micromanipulation test-beds. The μ VBFs was specifically designed to provide sub- μ N level force resolution in three dimensions. The 3D vision tracking algorithm is able to accurately measure the deflections of the PDMS compliant structure and compute the pushing forces, while running off-line at 15 Hz. This design was then used in two case studies to showcase some of its possible applications. It was able to manipulate a silicon micro-block while measuring forces in three dimensions. It also measured the surface forces encountered by the micro-part on different substrates. The μ VBFs design is a usable tool for force-controlled micromanipulation and assembly tasks that require 3D force sensing with sub- μ N resolution. Future work to obtain the 3D force information in real time is planned to enable this.

ACKNOWLEDGEMENTS

The authors acknowledge the facility access at Purdue University's Birck Nanotechnology Center, the 3D printer access and assistance from Dr. T. Siegmund, and the assistance of C. Bi for graphic assessment.

REFERENCES

- [1] F. Beyeler, S. Muntwyler, Z. Nagy, S. Muntwyler, F. Beyeler, and B. J. Nelson, "Three-axis micro-force sensor with sub-micro-Newton measurement uncertainty and tunable force range Related content Design and calibration of a MEMS sensor for measuring the force and torque Three-axis micro-force sensor with sub-micro-Newton measurement ,," *JOURNAL OF MICROMECHANICS AND MICROENGINEERING J. Micromech. Microeng.*, vol. 20, p. 8, 2010.
- [2] M. Rakotondrabe and I. A. Ivan, "Development and force/position control of a new hybrid thermo-piezoelectric microgripper dedicated to micromanipulation tasks," *IEEE Transactions on Automation Science and Engineering*, vol. 8, pp. 824–834, Oct 2011.
- [3] G. Wang and Q. Xu, "Design and precision position/force control of a piezo-driven microinjection system," *IEEE/ASME Transactions on Mechatronics*, 2017.
- [4] A. Hoover and R. Fearing, "Rapidly prototyped orthotweezers for automated microassembly," in *Proc. of IEEE International Conference on Robotics and Automation (ICRA)*, 2007.
- [5] Y. M. Efremov, W.-H. Wang, S. D. Hardy, R. L. Geahlen, and A. Raman, "Measuring nanoscale viscoelastic parameters of cells directly from AFM force-displacement curves OPEN,"
- [6] S. Guo, X. Zhu, D. Jańczewski, S. Siew Chen Lee, T. He, S. Lay Ming Teo, and G. Julius Vancso, "Measuring protein isoelectric points by AFM-based force spectroscopy using trace amounts of sample," *NATURE NANOTECHNOLOGY* I, vol. 11, 2016.
- [7] P. Hersen and B. Ladoux, "Biophysics: Push it, pull it," *Nature*, vol. 470, pp. 340–341, February 2011.
- [8] J. E. Pomeroy, H. X. Nguyen, B. D. Hoffman, and N. Bursac, "Genetically Encoded Photoactuators and Photosensors for Characterization and Manipulation of Pluripotent Stem Cells," *Theranostics*, vol. 7, no. 14, pp. 3539–3558, 2017.
- [9] J. P. Desai, A. Pillarisetti, and A. D. Brooks, "Engineering approaches to biomanipulation," *Annual Review of Biomedical Engineering*, vol. 9, pp. 35–53, August 2007.
- [10] A. Bolopion and S. Régner, "A Review of Haptic Feedback Teleoperation Systems for Micromanipulation and Microassembly Aude Bolopion, Stéphane Régner. A Review of Haptic Feedback Teleoperation Systems for Microma-nipulation and Microassembly. IEEE Transactions A Review of Haptic Feedback Teleoperation Systems for Micromanipulation and Microassembly," *Tech. Rep.* 3, 2013.
- [11] V. Venkatesan and D. J. Cappelleri, "Path Planning and Micromanipulation Using a Learned Model," *IEEE Robotics and Automation Letters*, 2018.
- [12] Y. Fujii, "Mechanical Systems and Signal Processing Method for generating and measuring the micro-Newton level forces," *Mechanical Systems and Signal Processing*, vol. 20, pp. 1362–1371, 2006.
- [13] Y. Fujii, K. Maru, D.-W. Shu, B. Gu, T. Yamaguchi, R. Lu, T. Jutanggoon, and P. Yupapin, "Material tester with static and dynamic micro forces," *Physics Procedia*, vol. 2, pp. 5–11, 2009.
- [14] M. A. Greminger and B. J. Nelson, "Vision-based force measurement," *IEEE Transactions on Pattern Analysis and Machine Intelligence*, vol. 26, no. 3, pp. 290–298, 2004.
- [15] F. M. Sasoglu, A. J. Bohl, and B. E. Layton, "Design and microfabrication of a high-aspect-ratio PDMS microbeam array for parallel nanonewton force measurement and protein printing," *Journal of Micromechanics and Microengineering*, vol. 17, pp. 623–632, 3 2007.
- [16] W. Jing, S. Chowdhury, M. Guix, J. Wang, Z. An, B. V. Johnson, and D. J. Cappelleri, "A Microforce-Sensing Mobile Microrobot for Automated Micromanipulation Tasks," *IEEE Transactions on Automation Science and Engineering*, pp. 1–13, 2018.
- [17] D. J. Cappelleri, G. Piazza, and V. Kumar, "A two dimensional vision-based force sensor for microrobotic applications," *Sensors & Actuators: A. Physical*, vol. 171, pp. 340–351, 2011.
- [18] S. D. Bhargav, N. Jorapur, and G. Ananthasuresh, "Micro-scale composite compliant mechanisms for evaluating the bulk stiffness of mcf-7 cells," *Mechanism and Machine Theory*, vol. 91, pp. 258 – 268, 2015.
- [19] A. Lukežić, T. Vojíř, L. Čehovin Zajc, J. Matas, and M. Kristan, "Discriminative Correlation Filter Tracker with Channel and Spatial Reliability," *International Journal of Computer Vision*, vol. 126, no. 7, pp. 671–688, 2018.
- [20] M. Guix, J. Orozco, M. Garcia, W. Gao, S. Sattayasamitsathit, A. Merkoči, A. Escarpa, and J. Wang, "Superhydrophobic alkanethiol-coated microsubmarines for effective removal of oil," *ACS Nano*, 2012.